Robotica (2003) volume 21, pp. 143–152. © 2003 Cambridge University Press
DOI: 10.1017/S0263574702004563 Printed in the United Kingdom

Effects of terrain irregularities on wheeled mobile robot

Maria Prado, Antonio Simón, Ana Pérez and Francisco Ezquerro

Department of Mechanical Engineering, University of Málaga, Campus El Ejido, 29103 Málaga (Spain)
E-mail: mpn@uma.es

(Received in Final Form: September 24, 2002)

SUMMARY
The influence of ground irregularities on the behavior of a wheeled mobile robot (WMR) navigating on uneven surfaces is addressed. The paper studies the vibratory movements induced on the body of the WMR, in order to analyze its ability for carrying out on-board tasks, and on the accuracy of the data collected by its external sensorial systems. The adhesion capability of the wheels of the WMR on this uneven terrain is also studied, since it conditions the braking, traction and steering performance. The method is applied to the WMR RAM.

KEYWORDS: Mobile robot; Ride analysis; Uneven terrain; External sensors; Dynamic performance.

1. INTRODUCTION

Mechanical vibrations on a wheeled mobile robot (WMR) influence the dynamic behavior of its sprung mass, the body of the robot, as well as the behavior of its unsprung mass, this mainly being the wheels of the robot. These factors tend to assume a greater significance with an increase in velocity for all mobile robots.

Both matters are addressed in this paper, since the dynamical movements of the body of the robot must be taken into account in order to study the on-board object manipulation ability, by checking the accuracy of the tasks carried out, and to assure the quality of the data acquired by external sensors linked to the sprung mass that could require its own suspension system. Regarding the unsprung masses, it is well known that the performance of the steering, driving and braking systems of a WMR are directly related to the maximum tangential forces available at the wheel-ground contact surface, and that these maximum forces can be computed as a function of:

- The adhesion and elastic characteristics of the wheels and of the ground; this can be assumed constant while the robot is navigating on the same terrain.
- The brake or traction torque commanded by the robot control.
- The lateral forces at the wheels related to the curvature of the path and the velocity of the robot, which is also commanded by its control.
- The forces normal to the ground at wheels; these are usually assumed to be constant by most WMR, but they experiment dynamical variations when navigating on uneven surfaces, even for stationary trajectories.

Mechanical vibrations in a WMR, i.e. Iow frequency vibrations, are mainly generated from two excitation sources: existing mobile elements within the robot and uneven rolling surfaces.

In the first group, the principal excitations are induced by the wheels and their associated elements and by the engine group and/or the transmission. However, for most WMR these mass groups are of a small size, and thus the related excitations have little influence, while it is the behavior of its driving and steering transmissions that result more significantly affected.

Regarding the second group, the ground vertical profile of the rolling surface on each wheel is the principal excitation source of the vehicle. The profile is usually modeled as random functions with Gaussian probability distributions, providing large local irregularities in the form of ramp or step functions which are added in order to simulate bumps, curbs . . . These are isolated and treated separately.[1] The roughness of the terrain is a broad band random function defined in terms of its statistics parameters, as the widely used spectral density, S_{zs}, which is generally described in terms of the spatial frequency, ν, in cycles per meter (in order to separate the collected data from the velocity of the vehicle used for the measurements).

The function S_{zs} is obtained from the analysis of each surface, but it has been observed that terrains of similar composition and structure present close values for this parameter.[2] Several studies[3–5] show a typical decrease of S_{zs} when ν increases, and a great similarity in the content of their frequency spectra on different rolling.[6] They show how wavelength and amplitude of the surface profile can be characterized by S_{zs} modeled as a decreasing function of $(\nu)^n$, with varying n values from 2 to 4. The maximum value of the function depends on the roughness of the modeled surface, but the slopes and inflection points remain constant. Moreover, in all models S_{zs} acquires greater values for all frequencies as the quality of the terrain decreases.

The aim of this paper is to describe a method to identify the main characteristics of the riding response of the body of a WMR and of its wheels when navigating on uneven terrains and, in particuiar, the statistical characteristics of the linear and angular vibration of its body and of the dynamic normal forces at its wheels as related to the adhesion capabilities. The method is focused on the WMR RAM.[7] For this purpose the paper is organized as follows: In Section 2 the spectral densities of the outputs from the transfer functions of the model and the spectral density of the excitations at wheels are evaluated; in Section 3 a

dynamic model of the WMR RAM to evaluate the transfer functions of interest is addressed; in Section 4 the spectral densities of the inputs are evaluated; in Section 5 the outputs of interest for RAM in two cases, when navigating on straight trajectories and when navigating in curved trajectories, are computed; in Section 6 the results computed with the approached method are shown and discussed and, finally, in Section 7 the conclusions of the paper are presented.

2. CHARACTERIZATION OF THE RIDING RESPONSE OF A WMR ON AN UNEVEN ROAD

Vertical surface profile can be expressed as a linear combination of shifted impulses, δ(t), therefore the excitation at the i-th wheel is given by:

$$zs_i(t) = \int_{-\infty}^{\infty} zs_i(\tau)\, \delta\,(t-\tau)\, d\tau \qquad (1)$$

The output $a_i(t)$, as the response of the variable a(t) to the excitation on the i-th wheel, is related to $zs_i(t)$ through the corresponding impulse response function, $h_i^a(\tau)$, in the convolution integral:

$$a_i(t) = \int_{\infty}^{\infty} h_i^a(\tau) zs_i(t-\tau)\, dt \qquad (2)$$

and, if the system is linear, the global response of a(t) to the excitations at all the wheels is given by:

$$a(t) = \sum_i \int_{\infty}^{\infty} h_i^a(\tau)\, zs_i(t-\tau)\, dt \qquad (3)$$

When the ground profile is modeled as a stationary random vibration with a Gauss distribution the mean excitation values are zero, and then the autocorrelation of the output can be evaluated as a function of the autocorrelation of the input; this is the case when the source of excitation is the ground roughness at the wheels of WMRs. Thus, naming R_{ii} to the autocorrelation of the function $zs_i(t)$ at the i-th wheel, the autocorrelation of the output a(t) of the robot model can be evaluated as:[8]

$$R_{aa}(\tau) = \sum_i \int_{\infty}^{\infty} \int_{\infty}^{\infty} h_i^a(\xi)\, h_i^a(\eta)\, R_{ii}(\tau-\xi-\eta)\, d\xi\, d\eta \qquad (4)$$

Since the ground is characterized by its spectral density, the relation input-output to be found is a relation between their respective spectral densities. As it is known, the Fourier transform of the impulse response is the transfer function between input and output in the frequency domain. Therefore, naming S_{AA} as the spectral density corresponding to the output a(t), $H_i^A(s)$ as the transfer function of this variable when excited by the input at the i-th wheels, $H_i^{A*}(s)$ as its complex conjugate, and $S_{ij}(s)$, for i=j as the spectral density of the ground excitation at the i-th wheel, and for i≠j as the cross spectral density between the inputs at i-th and the j-th wheels, from (4) it can be written:

$$S_A = \sum_{i=1}^{4} \sum_{j=1}^{4} H_i^{A*}\, S_{ij}\, H_j^A \qquad (5)$$

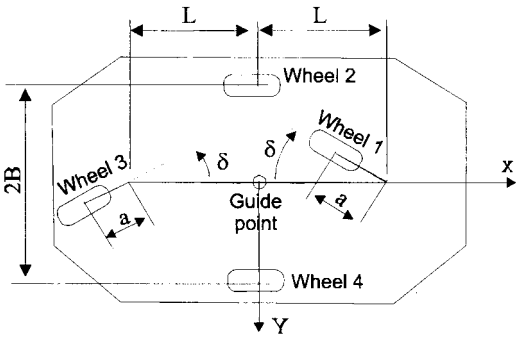

Fig. 1. Mechanical configuration of the WMR RAM.

3. DYNAMIC MODEL OF THE WMR RAM

RAM is a WMR designed for navigation with high maneuverability in indoor and outdoor industrial environments.[7] Its mechanical configuration consists of four wheels located at the vertices of a rhombus, one of whose diagonals is the longitudinal axis of the vehicle (see Figure 1). The two lateral wheels, wheels 2 and 4, are a semi-track B away from RAM's geometric center and are centered on the longitudinal axis of the robot, they are driven and unsteered parallel wheels. The front and rear wheels, wheels 1 and 3, are a semi-wheelbase L away from RAM's geometric center and are centered on its transverse axis. They are steering wheels. Completely independent servomechanisms power the two driven wheels. The two steering wheels are linked by a mechanical system that imposes steering angles of equal magnitude and opposite sign on both. Since the robot is only expected to have to negotiate small grades, it only incorporates suspension systems at the two lateral wheels. These are two independent spring/damper sets in parallel configuration.

The guide point of the robot is positioned at the cross point of its lateral and longitudinal axis, which coincides with the robot's gravity center (gc) and with its geometrical center in a plan view.

The dynamic model used for the study of the ride quality of RAM is fully approached in references [9, 10]. As a brief description, the robot is modeled as three concentrated masses shown in Figure 2: a mass M located at the gc of the sprung mass and with mass moment of inertia matrix $\bar{I}$; and two masses, $m_{ss}=[m_2\ m_4]^t$, located at the gc of the two semi-sprung masses.[11] Mass M has six degrees of freedom (dof) expressed by its linear velocity, $\vec{V}$, with three orthogonal components $[\dot{x}\ \dot{y}\ \dot{z}]$, and its angular velocity $\vec{\Omega}$ $[\dot{\varphi}\ \dot{\gamma}\ \dot{\theta}]$.

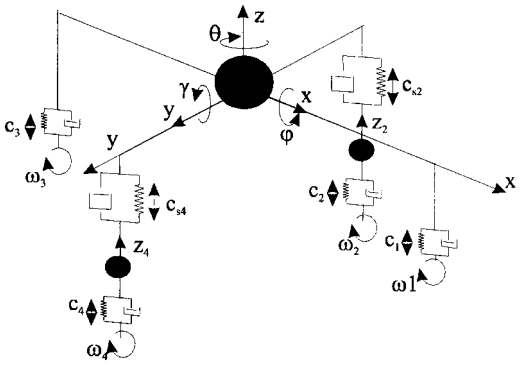

Fig. 2. Dynamic model of RAM and its state variables.

https://doi.org/10.1017/S0263574702004563 Published online by Cambridge University Press

While the motions of m_2 and m_4 are restricted to the displacement relative to M in the direction of the axis normal to the ground, their relative velocities are $z_s=[z_{s2}\ z_{s4}]^t$. Finally, there are four other masses located at the geometric center of each wheel, whose only dof is its angular velocity around the wheel's axis, $\omega=[\omega_1\ \omega_2\ \omega_3\ \omega_4]$, and with moment of inertia $I_\omega=[I_{\omega1}\ I_{\omega2}\ I_{\omega3}\ I_{\omega4}]$.

Each suspension system between M and m_{ss} is modeled by a spring-damper set in parallel configuration in the direction of the relative motions, $c_s=[c_{s2}\ c_{s4}]$ being the vector of the vertical compressions of suspension systems.

Regarding the rubber wheels, their behavior in normal; direction to the ground is modeled as a spring-damper set with constant coefficients[11], where $c=[c_1\ c_2\ c_3\ c_4]$ is the vector of the vertical compressions of wheels.

The excitation sources, as justified in Section 1, are the vertical profile of the rolling surface in contact with each of its four wheels, $\{zs_1(t), zs_2(t), zs_3(t), zs_4(t)\}$, respectively.

To study the ride quality of a WMR, only the pitch, roll, and bounce of the vehicle body and of its wheels with suspension have to be taken into consideration as dof. Thus for RAM the vector of the displacements of the state variables yields:

$$x(t)=[z_2(t)\ z_4(t)\ z\ (t)\ \varphi(t)\ \gamma(t)]^t \tag{6}$$

where the components of x(t), shown in Figure 2, are the bounce displacement of the wheels with suspension, $z_2(t)$ and $z_4(t)$, since it is the only movement with respect to the sprung mass allowed to the unsprung masses by the suspensions, and the bounce, z(t), pitch, $\varphi(t)$, and roll, $\gamma(t)$, displacement of the body of RAM.

To determine the transfer function for each variable of x(t) it is necessary to use a linearised model of RAM. For this purpose the model is linearised by neglecting the effect of gyroscopic moments and centrifugal forces acting on the gc of the robot, that are of low magnitude at the normally low navigating velocities of a wheeled robot, and by considering linear models for the tangential forces at the ground contact level, i.e. the longitudinal and lateral forces at wheel patches, which will not affect the ride behavior as argued below. Thus, the dynamic model of the WMR can be written as:

$$[M]\,\ddot{x}(t)+[C]\,\dot{x}(t)+[K]\,x(t)=u(t) \tag{7}$$

where [M] is the mass matrix, [C] the damping matrix, [K] the stiffness matrix and u(t) the excitation vector of the system from the ground profile.

The coefficients of the linearised dynamic model of Figure 2 take the form:[10,11]

K = Sim

$$\begin{Bmatrix}\begin{bmatrix} k_{r2}+k_{s2} & 0 & -k_{s2} & k_{s2}B & 0 \\ & k_{r4}+k_{s4} & -k_{s4} & -k_{s4}B & 0 \\ & & k_{r1}+k_{r3}+k_{s2}+k_{s4} & -(k_{s2}-k_{s4})B & -(k_{r1}-k_{r3})L \\ & & & (k_{s2}+k_{s4})B^2 & 0 \\ & & & & (k_{r1}+k_{r3})L^2 \end{bmatrix}\end{Bmatrix} \tag{8}$$

C = Sim

$$\begin{Bmatrix}\begin{bmatrix} R_{r2}+R_{s2} & 0 & R_{s2} & R_{s2}B & 0 \\ & R_{r4}+R_{s4} & R_{s4} & -R_{s4}B & 0 \\ & & (R_{r1}+R_{r3}+R_{s2}+R_{s4}) & -(R_{s2}\,R_{s4})B & -(R_{r1}-R_{r3})L \\ & & & (R_{s2}+R_{s4})B^2 & 0 \\ & & & & (R_{r1}+R_{r3})L^2 \end{bmatrix}\end{Bmatrix} \tag{9}$$

$$u(t)=\begin{bmatrix} -R_{r2}\dot{z}_{s2}-k_{r2}z_{s2}+m_2g \\ -R_{r4}\dot{z}_{s4}-k_{r4}z_{s4}+m_4g \\ -R_{r1}\dot{z}_{s1}-R_{r3}\dot{z}_{s3}-k_{r1}z_{s1}-k_{r3}z_{s3}+Mg \\ h\,\Sigma\,F_{yi} \\ L(R_{r1}\dot{z}_{s1}-R_{r3}\dot{z}_{s3}+k_{r1}z_{s1}k_{r3}z_{s3})+h\,\Sigma\,F_{\xi} \end{bmatrix} \tag{10}$$

$$M=\text{Diag}\,\{m_2,\ m_4,\ M,\ I_x,\ I_y\} \tag{11}$$

3.1. Transfer function for the movement of the WMR's body

To compute the transfer function of (5) when the output a(t) is one of the variables in the vector x(t) and the inputs are the ground irregularities, initially the Laplace transformation of model of (7) is evaluated assuming null initial conditions; thus the model in the s domain results in:

$$[M]\,s^2\,X(s)+[C]\,s\,X(s)+[K]\,X(s)=U(s)$$
$$\Rightarrow\ [T\,(s)]X\,(s)=U\,(s) \tag{12}$$

where:

$$[T(s)]=[M]s^2+[C]s+[K] \tag{13}$$

and:

$$\left.\begin{aligned} X(s)&=\mathcal{L}[x(t)] \\ U(s)&=\mathcal{L}[u(t)] \end{aligned}\right\} \tag{14}$$

Gravitational effects and the tangential forces at the wheel-ground contact are null, since they are not the vibratory excitation sources under study. Thus, the excitation vector, from (10), can be written as:

$$U(s)=[D][E]ZS(s) \tag{15}$$

where [D] is the matrix:

$$[D]=\begin{bmatrix} 0 & -1 & 0 & 0 \\ 0 & 0 & 0 & -1 \\ -1 & 0 & -1 & 0 \\ 0 & 0 & 0 & 0 \\ L & 0 & -L & 0 \end{bmatrix} \tag{16}$$

[E(s)] is a diagonal matrix including the elastic constants of the wheels:

$$[E(s)]=\text{Diag.}\,\{R_{r1}s+k_{r1},\ R_{r2}s+k_{r2},\ R_{r3}s+k_{r3},\ R_{r4}s+k_{r4}\} \tag{17}$$

and ZS(s) is the vector that sums up the surface profile spectra at wheels as:

$$ZS(s)=ZS_1(s)+ZS_2(s)+ZS_3(s)+ZS_4(s) \tag{18}$$

https://doi.org/10.1017/S0263574702004563 Published online by Cambridge University Press

where $ZS_i(s)$ is the vector that considers the excitation at the i-th wheel, written respectively as:

$$\begin{aligned} ZS_1(s) &= [ZS_1(s)\ 0\ 0\ 0]^t \\ ZS_2(s) &= [0\ ZS_2(s)\ 0\ 0]^t \\ ZS_3(s) &= [0\ 0\ ZS_3(s)\ 0]^t \\ ZS_4(s) &= [0\ 0\ 0\ ZS_4(s)]^t \end{aligned} \quad (19)$$

Therefore, the frequency response of the WMR in the studied dof when navigating on an uneven road, is obtained by substituting (15) into (12) as:

$$[X(s)] = [T(s)]^{-1}[D][E(s)]ZS(s) \quad (20)$$

And the transfer function between the variable at the k-th component of x(t) and the excitation at the i-th wheel is given by:

$$H_i^k(s) = \frac{X_k(s)}{ZS_i(s)} \quad (21)$$

computed after calculating the vector X(s), using equation (20), where $ZS_i(s)$ from (19) replaces ZS(s), where matrixes [T(s)], [D] and [E(s)] are introduced as previously described in (13), (16) and (17), respectively, and the denominator is given by (19).

3.2. Transfer functions for the forces normal to the wheel-ground contact

Regarding the performances of the systems of WMRs that interact with the environment through its wheels, steering, driving and braking systems, their dynamic behavior is directly related to the forces normal to the ground at the wheel patch, as was stated in Section 1.

The vertical behavior of elastic wheels was modeled as a linear spring in parallel with a damper[11]. Thus the normal force acting on each wheel-ground contact is given for all four wheels by:

$$f_z(t) = \begin{bmatrix} f_{z1}(t) \\ f_{z2}(t) \\ f_{z3}(t) \\ f_{z4}(t) \end{bmatrix} = \begin{bmatrix} R_{r1}\dot{c}_1(t) + k_{r1}c_1(t) \\ R_{r2}\dot{c}_2(t) + k_{r2}c_2(t) \\ R_{r3}\dot{c}_3(t) + k_{r3}c_3(t) \\ R_{r4}\dot{c}_4(t) + k_{r4}c_4(t) \end{bmatrix} \quad (22)$$

where R_{ri} is the vertical damping coefficient of the i-th wheel, k_{ri} is its vertical stiffness, and c_i is its vertical compression, as shown in Figure 2.

The transformation of (22) to the frequency domain, using the diagonal matrix [E] defined in (17) is:

$$F_z(s) = \begin{bmatrix} F_{z1}(s) \\ F_{z2}(s) \\ F_{z3}(s) \\ F_{z4}(s) \end{bmatrix} = \begin{bmatrix} (R_{r1}s + k_{r1})C_1(s) \\ (R_{r2}s + k_{r2})C_2(s) \\ (R_{r3}s + k_{r3})C_3(s) \\ (R_{r4}s + k_{r4})C_4(s) \end{bmatrix} = [E] \begin{bmatrix} C_1(s) \\ C_2(s) \\ C_3(s) \\ C_4(s) \end{bmatrix} \quad (23)$$

For the RAM model of Section 2 the compression vector, with [D] defined in (16), is given by:

$$[C_1(s)\ C_2(s)\ C_3(s)\ C_4(s)]^t = -[D]^t X(S) + ZS(s) \quad (24)$$

Thus, the normal contact forces can be written as:

$$F_z(s) = [E(s)]\,(ZS(s) - [D]^t X(s)) \quad (25)$$

By substituting the robot response calculated in (20) into (25), it results in:

$$F_z(s) = [E(s)]([I] - [D]^t[T(s)]^{-1}[D][E(s)])\ ZS(s) \quad (26)$$

where T(s) is the matrix given in (13).

The transfer function between the input in the i-th wheel and the normal contact force developed in the h-th wheel is obtained from expression (26) when ZS(s) is substituted by the corresponding excitation, as shown in (19), and rearranged:

$$H_i^{wh} = \frac{F_{zh}^i(s)}{ZS_i(s)} \quad (27)$$

where $F_{zh}^i(s)$ is the normal force at the patch of the h-th wheel when the i-th wheel is excited.

4. SPECTRAL DENSITIES AND CROSS SPECTRAL DENSITIES OF THE EXCITATION

To evaluate the robot response of (5), it is necessary to know, as well as the transfer functions (21) or (27):

(a) The spectral density of vertical profile of the rolling surface, S_{ii}: it has been extensively studied by different researchers, as it was described in Section 1, but it is most frequently described in terms of the spatial frequency, ν expressed in cycles/m as $s_{zs}(\nu)$; in robotics it is necessary to compute it as a function of the temporal frequency, or ω expressed in rad/s as $S^*_{zs}(\omega)$ or as f expressed in Hz as $S^{**}_{zs}(f)$, especially to evaluate the behavior of the sensorial systems or to suit the adhesion performances to the robot control characteristics. This change of variable is governed by the navigation velocity of the robot V, that relates the mentioned frequencies as:

$$\nu = \frac{\omega}{2\pi V} = \frac{f}{V} \quad (28)$$

Since the effective value of the signal must remain invariant under the change of variable, it must be verified that:

$$\int_0^\infty S_{zs}(\nu)\,d\nu = \int_{-\infty}^\infty S^*_{zs}(\omega)\,d\omega = \int_{-\infty}^\infty S^{**}_{zs}(f)\,df \quad (29)$$

Therefore by applying (28) to (29) it is found that:

$$S_{zs}(\nu) = 4\pi V\ S^*_{zs}(\omega) = V\ S^{**}_{zs}(f) \quad (30)$$

And these are the spectral densities of the inputs at wheels, thus:

$$S_{ii} = S^*_{zs}(\omega) \text{ or } S_{ii} = S^{**}_{zs}(f) \quad (31)$$

(b) The cross-spectral densities between wheel inputs. These will depend on the trajectory considered:

(1) 1f the robot navigates in a curved trajectory, it can be assumed that the inputs are not correlated, then:

$$S_{ij} = 0 \text{ for } i \neq j \quad (32)$$

(2) If the robot navigates in a straight trajectory, the input to wheels following the same track will be

https://doi.org/10.1017/S0263574702004563 Published online by Cambridge University Press

correlated, while there will not be a correlation between any other pair of inputs. For RAM, the only possible correlated input will be those of the rear and front wheels.

Some authors consider that a correlation exists between the inputs to wheels following parallel tracks.[8] But that is the case when the vehicle runs on a rolling surface generated as an isotropic bidimensional random process with circular symmetry from the unidimensional spectral density of any of the ground models mentioned in Section 1. However, the ground is not an isotropic surface, except in the case that the working distances are very short (less than two meters[12]), which does not occur for trajectories habitually planned by WMRs.

The cross-spectral density between excitations on the rear and front wheels of RAM is determined as the Fourier transform of its correlation, R_{13}, as:

$$S_{13}(\omega)=\frac{1}{2\pi}\int_{\infty}^{\infty} R_{13}\, e^{-j\omega t}\, dt \tag{33}$$

While R_{13} is given by:

$$R_{13}(\tau)=\lim_{T\to\infty}\frac{1}{T}\int_{0}^{T} zs_1(t)\, zs_3(t+\tau)\, dt \tag{34}$$

where the ground excitation on the front and the rear wheels is given by the same function but shifted a distance equal to the vehicle wheelbase, 2L. Thus, when the robot navigates at a velocity V, these functions result in:

$$zs_1(x)=zs_3(x+2L)\Rightarrow zs_3(t+\tau)=zs_1\left(t+\tau\frac{2L}{V}\right) \tag{35}$$

Therefore:

$$R_{13}(\tau)=\lim_{T\to\infty}\left(\frac{1}{T}\int_{0}^{T} zs_1(t)\, zs_3\left(t\frac{2L}{V}+\tau\right)dt\right)$$

$$\Rightarrow R_{13}(\tau)=R_{11}\left(\tau\frac{2L}{V}\right) \tag{36}$$

By substituting the result in (33), the cross-spectral density equals the rolling surface spectral density phase shifted an angle equal to 2L/V:

$$S_{13}(\omega)=S_{11}(\omega)\, e^{i\,\omega\frac{2L}{V}} \tag{37}$$

Moreover, the cross spectral densities between these wheels, 1 and 3, will meet:[8]

$$S_{31}=S^{*}_{13} \tag{38}$$

5. SPECTRAL DENSITIES OF THE OUTPUTS

By introducing the spectral densities obtained and cross spectral densities of the excitations in (5) and developing the result of (21) for each of the components of the movements studied into the vector x(t), on one hand, and the result of (27) for a generic h-th wheel on the other, the following results are found:

5.1. Navigation on a straight trajectory

The resulting spectral densities for bounce, pitch and roll of the robot body and for the normal forces at its wheels are, respectively:

$$\begin{aligned}
S_z&=\sum_{i=1}^{4} H_i^{z*}\, S_{ii}\, H_i^{z}+(H_1^{z*}\, S_{13}\, H_3^{z}+H_3^{z*}\, S_{31}\, H_1^{z})\\
&=\sum_{i=1}^{4} H_i^{z*}\, S_{ii}\, H_i^{z}+(H_1^{z*}\, S_{13}\, H_3^{z}+H_3^{z*}\, S^{*}_{13}\, H_1^{z})\\
S_\varphi&=\sum_{i=1}^{4} H_i^{\varphi*}\, H_i^{\varphi}\, S_{ii}+(H_1^{\varphi*}\, S_{13}\, H_3^{\varphi}+H_3^{\varphi*}\, S_{31}\, H_1^{\varphi})\\
&=\sum_{i=1}^{4} H_i^{\varphi*}\, H_i^{\varphi}\, S_{ii}+(H_1^{\varphi*}\, S_{13}\, H_3^{\varphi}+H_3^{\varphi*}\, S^{*}_{13}\, H_1^{\varphi})\\
S_\gamma&=\sum_{i=1}^{4} H_1^{\gamma*}\, H_1^{\gamma}\, S_{ii}+(H_1^{\gamma*}\, S_{13}\, H_3^{\gamma}+H_3^{\gamma*}\, S_{31}\, H_1^{\gamma})\\
&=\sum_{i=1}^{4} H_1^{\gamma*}\, H_1^{\gamma}\, S_{ii}+(H_1^{\gamma*}\, S_{13}\, H_3^{\gamma}+H_3^{\gamma*}\, S^{*}_{13}\, H_1^{\gamma})\\
S_{wh}&=\sum_{i=1}^{4} H_i^{wh*}\, H_i^{wh}\, S_{ii}+(H_1^{wh*}\, S_{13}\, H_3^{wh}+H_3^{wh*}\, S_{31}\, H_1^{wh})\\
&=\sum_{i=1}^{4} H_i^{wh*}\, H_i^{wh}\, S_{ii}+(H_1^{wh*}\, S_{13}\, H_3^{wh}+H_3^{wh*}\, S^{*}_{13}\, H_1^{wh})
\end{aligned} \tag{39}$$

Which is further simplified considering that the transfer functions for the RAM prototype meet:

$$\begin{aligned}
&H_1^{z}=H_3^{z}\ ;\ H_1^{\varphi}=-H_3^{\varphi}\ ;\ H_1^{\gamma}=-H_3^{\gamma}\\
&H_2^{z}=H_4^{z}\ ;\ H_2^{\varphi}=-H_4^{\varphi}\ ;\ H_2^{\gamma}=-H_4^{\gamma}
\end{aligned} \tag{40}$$

Then (39) can be rewritten as:

$$\begin{aligned}
S_z&=\sum_{i=1}^{4} H_i^{z*}\, S_{ii}\, H_i^{z}+H_1^{z*}(S_{13}+S^{*}_{13})\, H_1^{z}\\
S_\varphi&=\sum_{i=1}^{4} H_i^{\varphi*}\, S_{ii}\, H_i^{\varphi}+H_1^{\varphi*}(S_{13}+S^{*}_{13})\, H_1^{\varphi}\\
S_\gamma&=\sum_{i=1}^{4} H_1^{\gamma*}\, S_{ii}\, H_1^{\gamma}+H_1^{\gamma*}(S_{13}+S^{*}_{13})\, H_1^{\gamma}\\
S_{wh}&=\sum_{i=1}^{4} H_i^{wh*}\, S_{ii}\, H_i^{wh}+H_1^{wh*}\, S_{13}\, H_3^{wh}+H_3^{wh*}\, S^{*}_{13}\, H_1^{wh}
\end{aligned} \tag{41}$$

https://doi.org/10.1017/S0263574702004563 Published online by Cambridge University Press

5.2. Navigation on a curved trajectory

In these cases the spectral densities of the outputs can be evaluated by:

$$S_z = \sum_{i=1}^{4} H_i^{z*}\, S_{ii}\, H_i^{z}$$

$$S_\varphi = \sum_{i=1}^{4} H_i^{\varphi*}\, S_{ii}\, H_i^{\varphi} \qquad (42)$$

$$S_\gamma = \sum_{i=1}^{4} H_i^{\gamma*}\, S_{ii}\, H_i^{\gamma}$$

$$S_{wh} = \sum_{i=1}^{4} H_i^{wh*}\, S_{ii}\, H_i^{wh}$$

6. RESULTS

Several experimental studies of the statistical characterization of the ground vertical profile in most terrains can be found in the literature,[1–5] the different measurements yielding very similar conclusions, as stated in Section 1. For the scope of this paper, the ground vertical profile proposed by Anon[3] for a standard roadway was used as an excitation input to the model of RAM, although functions for evaluating surface vertical profile on other types of terrain and with expressions proposed by other authors have been corroborated showing similar results.

6.1. Study of the WMR body behavior

The characteristics of the movements of the RAM's body found by applying the method described in this paper are presented and discussed in this Section, firstly for curved trajectories and, later, analyzing the distinctive results on straight paths.

6.1.1. Navigation on curved trajectories. Figure 3 shows the temporal frequency response for the bounce, roll and pitch of the RAM at three different navigation velocities. It is observed that faster velocities generate higher spectral densities, all cases exhibiting a characteristic monotonical decrease when f is increased. If the outputs are expressed in terms of the spatial frequency of the ground excitation, ν, then S_z, S_φ and S_γ would remain constant, but this is not a result of interest since the data collected by the electronic sensors of WMRs or used by their controls, depend on their sample frequency disregarding the navigation velocity.

Figure 4 shows the modulus of the transfer function for each dof. The influence of the natural frequencies of the robot body of RAM[9,10] (11.2 Hz for bounce, 13.8 Hz for roll and 1.5 Hz for pitch) can be recognized; each movement is obviously mainly influenced by its own natural frequency. The figure shows that for the configuration of RAM, roll is only induced by the lateral wheels (with suspension); thus the axis normal to the one that links them is the roll axis of the robot, i.e. its longitudinal axis; while pitch is only generated by the central wheels of RAM (without

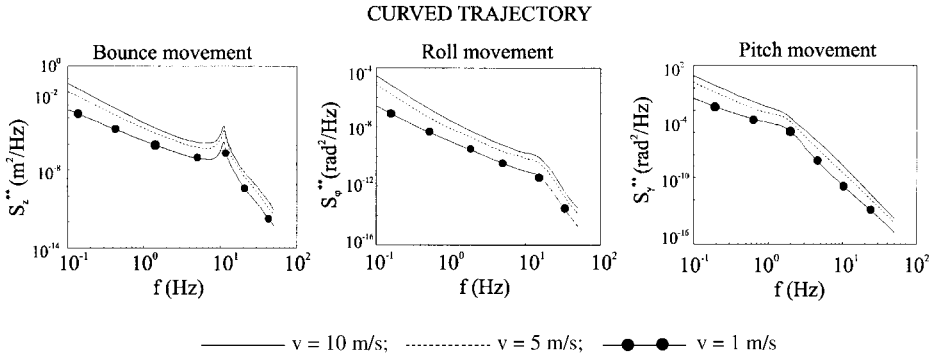

Fig. 3. Spectral density of the movements of the RAM's body at different navigation velocities on curved trajectories.

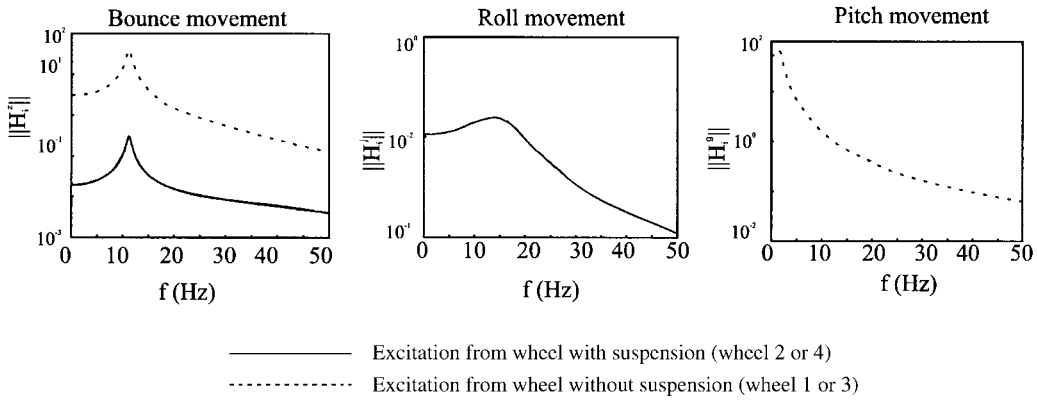

Fig. 4. Modulus of the transfer function between the movements of the RAM's body and the excitation at the i-th wheel.

https://doi.org/10.1017/S0263574702004563 Published online by Cambridge University Press

suspension), thus the axis normal to the one that links them is its pitch axis of the robot, i.e. its transversal axis.

It is also observed in this figure that the angular movement generated by the wheels with suspension, has lower transmissibility than the one generated through suspension systems. Obviously the suspension systems damp the excitation.

It is usual to study mechanical vibrations of vehicles in terms of their root mean square value (RMS). To make the evaluation of the RMS possible of the movements caused by ground irregularities, it is necessary to select a lower bound for the frequency of excitation, since S_{zs} tends to infinity when ν tends to zero. This lower frequency is chosen as a function of the robot wheelbase as in reference [1]:

$$\nu_{\text{lim}} = \frac{N}{2L};\ N = 4 \tag{43}$$

As an example, in Figure 5 the RMS of the vertical movement generated by bounce, roll and pitch of the most distant point from the gc of RAM (the cross point of the roll and pitch axis of the robot)[9] is plotted. All displacements present an increasing linear rate law with the navigation velocity. Again, the highest importance of the bounce movements and the lowest magnitude of roll movements are shown.

These results show that it is important to carefully select the location of the external sensors in order to improve the accuracy of the data collection. For this example, it is obvious that positions close to the roll, and above all to the pitch axis, imply smaller movements than positions far from it, but this is not an important point since the major disturbances are caused by the bounce movements, especially at high velocities, even at the most distant point from the axis.

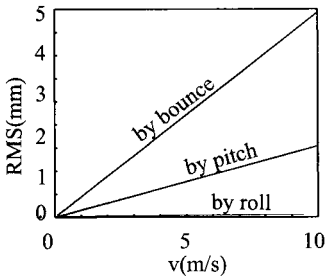

Fig. 5. Movement of the most distant point from the pitch and roll axis vs navigation velocity.

6.1.2. Navigation on straight trajectories. Figure 6 displays the spectral density when the rear and front wheels run along the same track. The results are similar to those of Section 6.1.1., but bounce and pitch exhibit the effect of the correlation between the wheels that run on the same track. This correlation does not influence roll movements because they are induced only by the lateral wheels of RAM that always run on different tracks.

Because of this wheelbase coupling, the value of Sz reaches a local maximum at the frequencies for which the excitations on rear and front wheels are in phase and a local minimum when they are in antiphase, yet S_γ shows the inverse effect. Thus the local maxima are located at frequencies dependent on the navigation velocity, namely:

$$\left.\begin{aligned} f^{\text{coupling}}_{\text{bounce}} &= \frac{N}{2L}V \\ f^{\text{coupling}}_{\text{pitch}} &= \frac{2N+1}{2\cdot 2L}V \end{aligned}\right\} \quad N = 1, 2, 3 \ldots \tag{44}$$

As an example, Figure 7 shows the RMS for both dof at the guide point on curved and on straight trajectories to point out the effect of the wheelbase coupling. It is observed that the magnitude of the bounce increases in straight paths and the magnitude of pitch decreases, facts that become more significant for high velocities. Thus for the configuration of RAM, when the fact under study is located at the guide point for low to moderate navigation velocities, it is sufficient to study the effect of uneven roads on curved trajectories, disregarding the wheelbase coupling phenomenon, since a less heavy movement is considered and the results would be using a safety factor greater than one. But it could be necessary to analyze straight trajectories for high velocities if the study demands exactitude.

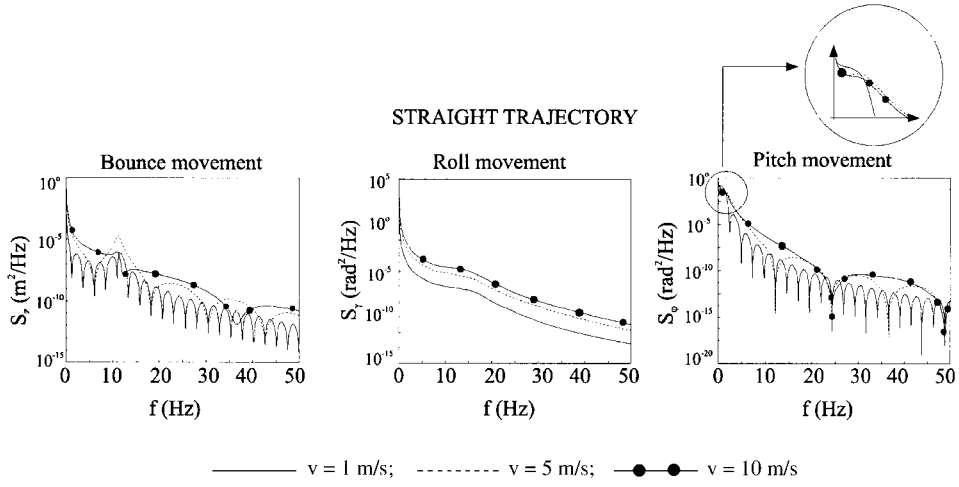

Fig. 6. Spectral density of the movements of the RAM's body at different navigation velocities on straight trajectories.

https://doi.org/10.1017/S0263574702004563 Published online by Cambridge University Press

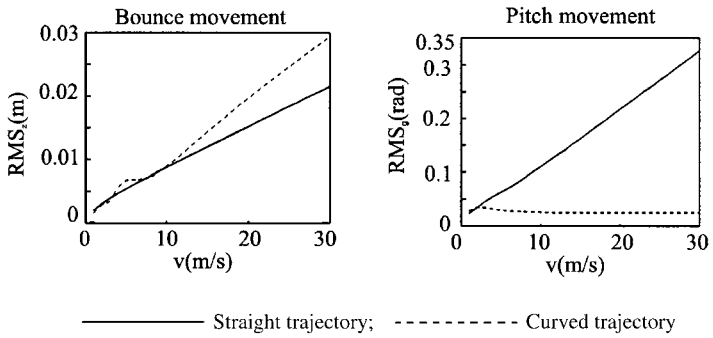

Fig. 7. Bounce and pitch of the guide point.

It is evident that the effects of ground irregularities on any other point of the body of the robot must be individually analyzed.

6.2. Study of the wheel-ground normal forces

As was explained in Section 1, the adherence capacity of the robot wheels and therefore the performances of its steering, braking or traction systems, are directly linked to the forces normal to the wheel patch. Therefore the dynamic magnitude of this load when navigating on uneven roads must be analyzed.

The mechanical configuration of RAM makes its wheels exhibit longitudinal and transversal symmetrical results when the ground unevenness is studied. Therefore the results presented in this Section refer only to a driven wheel or wheel without suspension, that represents or rear or front wheel, and to a steering wheel or wheel with suspension, that represents or left or right wheel.

6.2.1. Navigation on curved trajectories. Figure 8 shows the frequency response of the normal loads on driven and steering wheels for three navigation velocities. It is observed that the higher the robot velocity, the higher the spectral density at low frequencies for the region that influences the adherence capacity. It is also observed that, as well as for low frequencies, the major values of S_{wh} appear around the natural frequencies of the wheels (11.2 Hz for a wheel without suspension and 9.7 Hz for a wheel with suspension)[9]. As expected, the suspension systems damp S_{wh} at driven wheels and the maximum value of the spectral density is lower than for wheels without suspension.

To study the dynamic performance of the WMR, a dynamic load factor for its wheels, DLF, is evaluated as the ratio of the RMS of the dynamic load to the static load on the wheel, using the threshold for ν_{lim} of (43). Figure 9 shows the results versus navigation velocity. It is observed that DLF increases with V presenting two differentiated regions:

- For low velocity: DLF is approximately a quadratic function of V and its magnitude is lower for driven than for steered wheels.
- For high velocity: DLF is approximately a linear function of V and its magnitude is higher for driven than for steered wheels. This is because the suspension systems make the navigation smoother for the body motion but they allow the driven wheels to be unloaded. However, it must be said that the robot dynamic model of this paper does not take into account the possible separation of the wheel from the ground, and this fact is likely to occur at high velocities in wheels without a suspension system.

Vibratory effects with DLF lower than 20% are not expected to reduce the adherence capacity of a wheel, and the influence of the ground irregularities can be neglected for RAM at not very high velocities (not available at present).

6.2.2. Navigation on straight trajectories. Figure 10 shows the spectral density of normal loads on wheels for the robot running on a straight trajectory. The results are similar to that of Section 6.2.1. but there is a ripple superimposed that is generated by the wheelbase coupling; the event is less important for wheels where the suspension system smoothes the resonance peaks caused by the coupling.

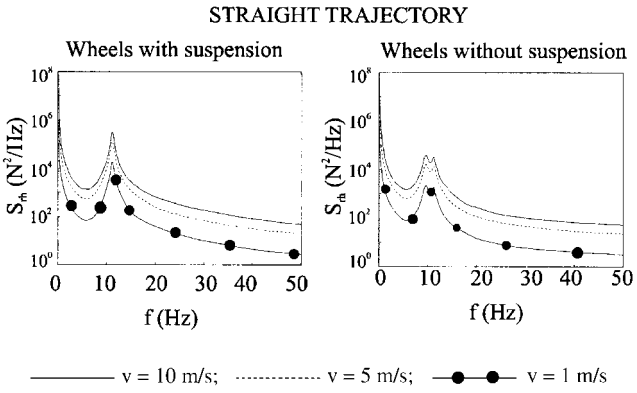

Fig. 8. Spectral density of the normal load at the wheel contact at different navigation velocities on curved trajectories.

https://doi.org/10.1017/S0263574702004563 Published online by Cambridge University Press

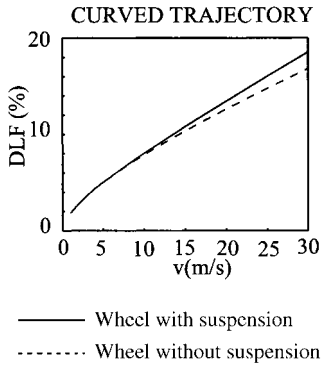

Fig. 9. DLF of RAM's wheels vs navigation velocity.

The consequence of the coupling is clearer in Figure 11 which plots DLF versus robot velocity. It can be seen that the velocities which decrease the magnitude of DLF for the wheels without suspension, increase this factor for the wheels with suspension, and vice versa. But the wheelbase coupling phenomenon is not very significant in any case and it can be disregarded when evaluating the performances of the wheels of RAM.

7. CONCLUSIONS

This paper deals with a linearized dynamic model of a WMR to analyze, on one hand, the frequency response of the body movements, bounce, pitch and roll, since they condition the on-board ability and accuracy of the data collected by the external sensorial system and, on the other hand, the frequency response of the forces normal to the wheel-ground contact, since it can condition the performances of the steering, braking and traction systems. The mechanical vibrations are generated by the ground roughness when the robot is navigating on uneven terrain, the major vibratory excitation source for WMR. These irregularities are characterized by the spectral density of the rolling surface vertical profile.

For this purpose, the transfer functions between each output of interest and the vertical displacement of the wheels are evaluated for the WMR RAM as well as the spectral densities and cross spectral densities of the excitations, distinguished when the robot navigates on curved or straight trajectories. These spectral densities are expressed in terms of sample frequency from the extensive experimental data available in the literature for the vertical profile of several terrains.

From the results presented in the paper regarding the dynamic behavior of the body of the robot it can be concluded that the most important vibrations are of low frequency and that their magnitude increase when the navigation velocity increases. As expected, it is also observed that the movements of the body generated by the wheels with suspension are lower than when this system is not built in the excited wheel. But not all the dofs have the same degree of effect on the behavior of a specific point of the body, so the location of the point of interest must be specifically studied in order to analyze how any improve-

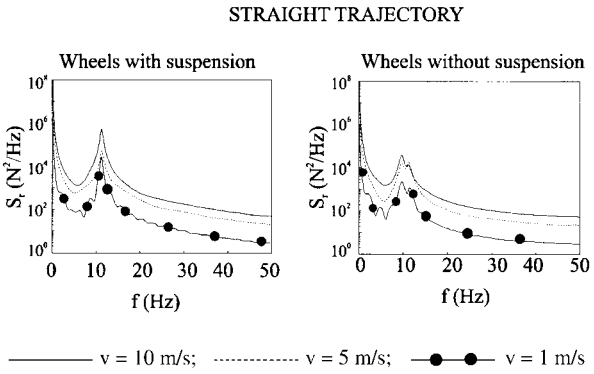

Fig. 10. Spectral density of the normal load at the wheel contact at different navigation velocities on straight trajectories.

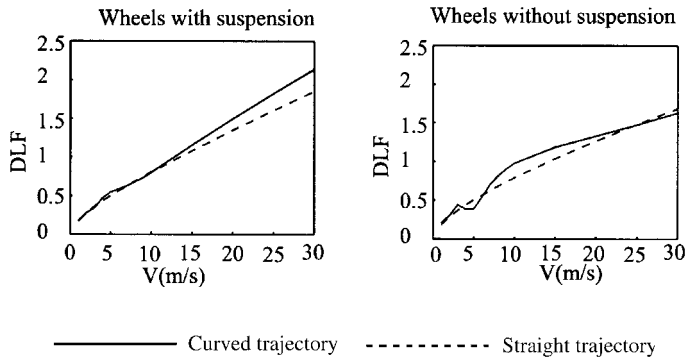

Fig. 11. DLF of RAM's wheels vs navigation velocity on curved and on straight trajectories.

https://doi.org/10.1017/S0263574702004563 Published online by Cambridge University Press

ment on the suspension system can influence its dynamic performances.

When straight trajectories are analyzed a wheelbase coupling phenomenon is observed, that generates a ripple in the spectral density of bounce and pitch at frequencies depending on the navigation velocity. This result demonstrates the need of avoiding those navigation velocities that generate frequencies of excitation at the peaks of the frequency response: An important fact when the robot navigates on rolling surfaces with continuously distributed irregularities.

Regarding the dynamic normal loads on wheels, the paper shows that the RMS of their spectral density also increases with the navigation velocity. Their major magnitude appears at low frequencies and especially around the bounce natural frequency of the robot body for the configuration of RAM.

The dynamic load factor (DLF) has been computed for all wheels to evaluate the influence of the road irregularities on their adhesion capability. The results indicate that it increases as a linear function of the robot velocity for slow trajectories and as a quadratic function for fast trajectories. But the values always remain low enough to be disregarded as an influence on uneven terrains when evaluating the traction, braking or maneuverability capacity for the navigation velocities of RAM on standard roads. Any other case must be studied in the way approached in the paper.

In straight trajectories, the wheelbase coupling between wheels that follow the same track modifies the DLF, mainly in wheels without suspension. The results indicate that the performance and maneuverability of WMRs must take into account the road roughness mainly when they navigates at high velocities, but they allow the authors to neglect the phenomenon for the case studied.

8. References

1. D. Cebon, *Handbook of Vehicle-Road Interaction* (Swets & Zeitlinger Publishers, The Netherlands, 2000).
2. R. P. La Barre, "The Measurement and Analysis of Road Surface Roughness," *Motor Industry Research Association, Report* 1970/5 (1969).
3. D. Anon, "Proposal for Generalised Road Input to Vehicles," *ISO/TC 108/WGp* draft No.3e (1972).
4. L. Segel, *The Mechanics of Heavy-Duty Trucks and Truck Combinations* (The Open University, U.K, 1987).
5. T. D. Gillespie, *Fundamentals of Vehicle Dynamics* (Society of Automotive Engineers, USA, 1994).
6. A. N. Heath, "Modelling and Simulation of Road Roughness," *Proc. 11th IAVSD Symposium on the Dynamics of Vehicle on Roads and on Railway Tracks* (1987) pp. 275–284.
7. A. Ollero, A. Simón, F. Garcia and V. Torres, "Integrated Mechanical Design and Modelling of a New Mobile Robot," **In**: *Intelligent Components and Instruments for Control and Applications* (Pergamon Press, USA, 1993).
8. D. E. Newland, *Random Vibrations, Spectral & Wavelet Analysis* (Longman, UK, 1993).
9. M. Prado, "Dynamic modelling of mobile robot. Application to trajectory planning," *PhD Thesis* (University of Málaga, Málaga, Spain, in Spanish, 2000).
10. M. Prado, A. Simón and F. Ezquerro, "Velocity, acceleration and deceleration bounds for a time-optimal planner of a wheeled mobile robot," *Robotica* **20** Part 2, 181–193 (2002).
11. A. Gentile, A. Messina and A. Trentadue, "Dynamic Behaviour of a Mobile Robot Vehicle with a Two Caster and two Driving Wheel Configuration," *Vehicle System Dynamics* **25**, 89–112 (1996).
12. M. S. A. Hardy and D. Cebon, "The Response of a Flexible Pavement to Moving Dynamics Loads," *Proc. Institute of Acoustics* **10**(2), 485–492 (1988).

https://doi.org/10.1017/S0263574702004563 Published online by Cambridge University Press